LETTER

doi:10.1038/nature24999

Black-hole-regulated star formation in massive galaxies

Ignacio Martín-Navarro[1,2], Jean P. Brodie[2], Aaron J. Romanowsky[1,3], Tomás Ruiz-Lara[4,5] & Glenn van de Ven[2,6]

Supermassive black holes, with masses more than a million times that of the Sun, seem to inhabit the centres of all massive galaxies[1,2]. Cosmologically motivated theories of galaxy formation require feedback from these supermassive black holes to regulate star formation[3]. In the absence of such feedback, state-of-the-art numerical simulations fail to reproduce the number density and properties of massive galaxies in the local Universe[4–6]. There is, however, no observational evidence of this strongly coupled coevolution between supermassive black holes and star formation, impeding our understanding of baryonic processes within galaxies. Here we report that the star formation histories of nearby massive galaxies, as measured from their integrated optical spectra, depend on the mass of the central supermassive black hole. Our results indicate that the black-hole mass scales with the gas cooling rate in the early Universe. The subsequent quenching of star formation takes place earlier and more efficiently in galaxies that host higher-mass central black holes. The observed relation between black-hole mass and star formation efficiency applies to all generations of stars formed throughout the life of a galaxy, revealing a continuous interplay between black-hole activity and baryon cooling.

As shown in Fig. 1, the mass of supermassive black holes ($M_\bullet$) scales with the stellar velocity dispersion (σ) of their host galaxies[2,7]. The scatter in this relation can be used to quantify how massive a given black hole is compared with the average population. We can then define over-massive and under-massive black-hole galaxies as those objects lying, respectively, above and below the best-fitting relation between $M_\bullet$ and σ. In other words, over-massive black-hole galaxies have central black holes more massive than expected, whereas under-massive black-hole galaxies host relatively light supermassive black holes. The distinction between these two types of galaxy allows us to evaluate the role of black-hole activity in star formation, as the amount of energy released into a galaxy is proportional to the mass of the black hole[8,9].

We based our stellar population analysis on long-slit optical spectra from the Hobby–Eberly Telescope Massive Galaxy Survey (HETMGS)[10]. The resolution of the data varies between 4.8 Å and 7.5 Å, depending on the slit width. We adopted a fixed aperture of half the effective radius, $0.5R_e$, where R_e is defined as the galactocentric radius that encloses half of the total light of a galaxy. This aperture is large enough to allow a direct comparison in the future between our results and numerical simulations, but also small enough to ensure that we are dominated by *in situ* star formation[11]. The sizes of all galaxies in our sample were calculated in a homogeneous way using infrared *K*-band photometry[12]. We focused on spectroscopic analysis of wavelengths between 460 and 550 nm, covering the most prominent spectral features indicating age and metallicity in the optical range.

Star formation histories (SFHs) were measured using the Stellar Content and Kinematics via Maximum A Posteriori likelihood (STECKMAP) code[13], fed with the MILES stellar population synthesis models[14]. STECKMAP is a Bayesian method that decomposes the observed spectrum of a galaxy as a temporal series of single stellar population models. Its ability to recover reliable SFHs of unresolved systems has been thoroughly tested[15–17]. Furthermore, STECKMAP-based SFHs are in remarkable agreement with those based on colour–magnitude diagrams of nearby resolved systems[18]. Our SFHs are reliable in a relative sense (see Methods) even if there are systematics from the limited set of models.

Our final sample consists of all HETMGS galaxies for which there are direct measurements of black-hole masses, and for which we can also determine their SFHs. There are 74 in total, probing total stellar masses from $M \approx 1 \times 10^{10} M_\odot$ to $M \approx 2 \times 10^{12} M_\odot$, where $M_\odot$ is the mass of the Sun. We removed from the final sample galaxies with strong nebular emission lines, in particular around the optical Hβ line, which affected the quality of the STECKMAP fit. Galaxies with prominent emission lines populate only the low-σ end of our sample ($\log\sigma \lesssim 2$). We normalized individual SFHs so that each galaxy has formed one mass unit at redshift $z \approx 0$.

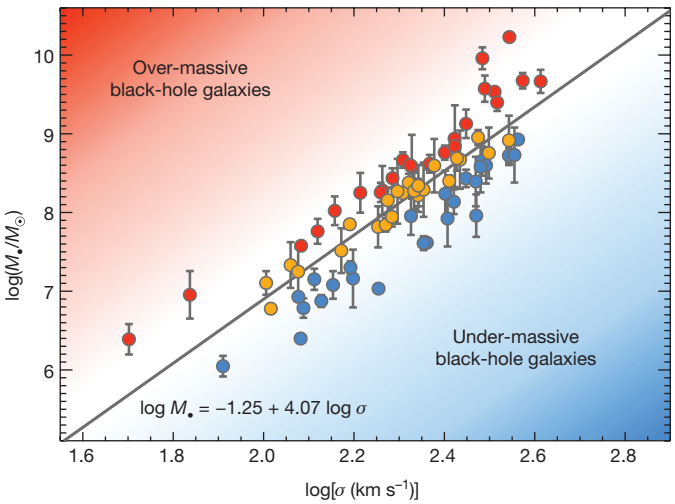

Figure 1 | Dispersion relation between black-hole mass and stellar velocity. The stellar velocity dispersion of galaxies (σ) tightly correlates with the mass of their supermassive black hole ($M_\bullet$). Data points correspond to the 74 HETMGS galaxies with measured black-hole masses and high-quality spectra. The solid line indicates the average black-hole mass for a given velocity dispersion. Galaxies more than +0.2 dex above this best-fitting $M_\bullet$–σ relation have black holes more massive than expected for their velocity dispersion, and therefore are called over-massive black-hole galaxies (red). Conversely, galaxies hosting less-massive black holes than the average population (by −0.2 dex or beyond) are called under-massive black-hole galaxies (blue). Galaxies with standard black-hole masses are shown in orange. Error bars are 1σ uncertainties.

[1]University of California Observatories, 1156 High Street, Santa Cruz, California 95064, USA. [2]Max-Planck Institut für Astronomie, Konigstuhl 17, D-69117 Heidelberg, Germany. [3]Department of Physics and Astronomy, San José State University, One Washington Square, San Jose, California 95192, USA. [4]Instituto de Astrofísica de Canarias, E-38205 La Laguna, Tenerife, Spain. [5]Departamento de Astrofísica, Universidad de La Laguna, E-38200 La Laguna, Tenerife, Spain. [6]European Southern Observatory, Karl-Schwarzschild-Strasse 2, 85748 Garching bei München, Germany.

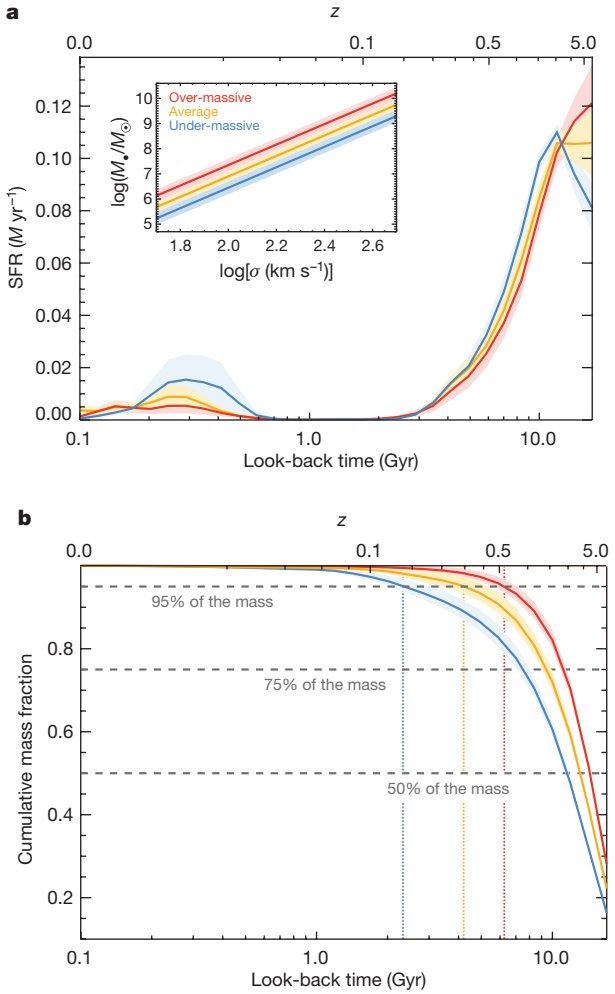

Figure 2 | Evolution of star formation over cosmic time. Red, orange and blue solid lines correspond to over-massive, standard and under-massive black-hole galaxies, respectively. Shaded regions indicate 1σ uncertainties in the mean values (but not model uncertainties). M, normalized mass. **a**, The evolution of the star formation rate (SFR) as a function of look-back time; **b**, the cumulative mass distribution for the three types of galaxy. Vertical dotted lines in **b** indicate when 95% of the final mass has been reached. The coupling between black-hole mass and star formation applies to all generations of stars, from those formed at $z \approx 5$ to the youngest generations. Our measurements of the SFH as a function of black-hole mass show how the latter drives baryonic cooling within massive haloes.

Our main result is summarized in Fig. 2, in which we show how star formation rates and cumulative stellar mass have evolved in over-massive (red), in standard (orange) and in under-massive (blue) black-hole galaxies. This evolution of star formation over cosmic time is strongly coupled to the mass of the central black hole. Galaxies with over-massive black holes experienced more intense star formation rates in the very early Universe (look-back times of 10 Gyr or more) than did galaxies with less-massive black holes. Star formation in over-massive black-hole galaxies was quenched earlier, with these galaxies reaching 95% of their final mass about 4 Gyr earlier, on average, than under-massive black-hole galaxies, as shown by the cumulative mass distributions. The amount of recent star formation, however, inversely correlates with the mass of the black holes: that is, young stellar populations are more prominent in under-massive black-hole galaxies. A Kolmogorov–Smirnov test of the distributions shown in Fig. 2 indicates that they are significantly different (P value of 0.026).

It is worth emphasizing that SFHs and black-hole masses are completely independent observables. Black-hole masses were calculated using a wide variety of methods but without detailed information on the stellar population properties[12]. If the differences presented in Fig. 2 were artefacts of the stellar population analysis, they could not be coupled to the mass of the black hole. This relative character of our approach minimizes the effect of systematic errors in the analysis. We have further checked that our choices for the STECKMAP free parameters do not affect our conclusions, and neither does the adopted $M_\bullet$–σ relation, nor the stellar population modelling (see Methods). Note also that there is no significant difference between the velocity dispersions of under-massive, standard and over-massive black-hole galaxies ($\log\sigma_{\rm under} = 2.32 \pm 0.04$, $\log\sigma_{\rm standard} = 2.30 \pm 0.03$, $\log\sigma_{\rm over} = 2.32 \pm 0.04$).

It could be argued that the process regulating black-hole growth also affected the efficiency of baryonic cooling within galaxies. In particular, objects formed in high-density environments could have grown more-massive black holes and formed their stellar populations differently owing to the amount and properties of the available gas. However, the lack of a morphological offset across the $M_\bullet$–σ relation[12,19] disfavours such a scenario (see also Methods). In addition, differences in formation timescales such as those shown in Fig. 2 do not depend on galaxy environment[20]. Thus, over-massive and under-massive black-hole galaxies have probably experienced similar formation paths. It is worth noting here the relative character of our analysis, that is, independent of the normalization of the $M_\bullet$–σ relation. Moreover, the robustness of our results with respect to additional parameters such as galaxy size or stellar density (see Methods) further indicates that galaxies with over-massive and under-massive black holes are different only in terms of their detailed stellar population properties and black-hole masses. Dynamically, morphologically and structurally, the two types of galaxy are indistinguishable.

The measurements shown in Fig. 2 probe the star formation processes within massive haloes since the early Universe. Interestingly, black-hole masses and star formation seem to be related as early as $z \approx 5$. This invalidates any scenario in which the observed scaling relations between black holes and host galaxies would emerge non-causally from the hierarchical evolution of a lambda cold-dark-matter (ΛCDM) Universe[21,22]. At the peak rate of star formation, baryon cooling was more efficient in galaxies with (present-day) more-massive black holes. The stellar mass formed around $z \approx 5$ in over-massive black-hole galaxies is about 1.3 times that formed in under-massive black-hole galaxies. Assuming the ratio of stellar mass to black-hole mass observed in the local Universe[12], these differences in the amount of stellar mass formed at $z \approx 5$ imply that more than 50% of the (vertical) scatter in the $M_\bullet$–σ relation results from this initial phase of galaxy formation and black-hole growth. We hypothesize that over-massive black-hole galaxies rapidly reached a black-hole mass capable of quenching star formation, which led to a shorter timescale for star formation. Thus, the baryon cooling efficiency at high redshift would play a major role in determining the present-day mass of supermassive black holes, feeding the primordial seeds of the black holes with gas, in agreement with quasar observations[23].

The importance of supermassive black holes in galaxy evolution arises from their potential role as quenching agents. We found that in those galaxies with less-massive central black holes, star formation lasted longer. This time delay, consistent with the observed differences in the abundance of alpha-process elements versus iron [α/Fe] of over-massive and under-massive black-hole galaxies[24], is naturally explained if quenching is driven by active galactic nucleus (AGN) feedback. Accretion onto higher-mass black holes leads to more energetic AGN feedback which would quench the star formation faster. This high-redshift picture has its $z \approx 0$ counterpart, as recent star formation is also expected to be regulated by AGN activity. If the rate of energy injection scales with the mass of the black hole[8,9], less-massive black holes, growing at low accretion rates in the nearby Universe, would be less efficient at keeping hot the gaseous corona, which will ultimately

cool and form new stars[25]. In Fig. 2, the fraction of young stars anti-correlates with the relative mass of the black hole, further supporting an active role of black holes in regulating star formation within massive galaxies.

Investigating the connection between star formation and black-hole activity has been one of the biggest observational challenges since AGNs were proposed as the main source of feedback within massive galaxies. Whereas star formation takes place over long periods of time, the rapid and nonlinear response of black holes to gas accretion[26] complicates a clean empirical comparison between AGN luminosity and star formation rate. AGNs typically populate star-forming galaxies, but their luminosities may not correlate with observed rates of star formation[27–30]. Here, we have made use of the relation between black-hole mass and SFHs to show that the evolution of star formation in massive galaxies over cosmic time is driven by black-hole activity. Our results indicate that there may be a causal origin for the observed scaling relations between galaxy properties and black-hole mass, offering observational support for AGN-based quenching mechanisms.

Online Content Methods, along with any additional Extended Data display items and Source Data, are available in the online version of the paper; references unique to these sections appear only in the online paper.

Received 23 May; accepted 28 October 2017.
Published online 1 January 2018.

1. Magorrian, J. *et al.* The demography of massive dark objects in galaxy centers. *Astron. J.* **115,** 2285–2305 (1998).
2. Gebhardt, K. *et al.* A relationship between nuclear black hole mass and galaxy velocity dispersion. *Astrophys. J.* **539,** L13–L16 (2000).
3. Silk, J. & Mamon, G. A. The current status of galaxy formation. *Res. Astron. Astrophys.* **12,** 917–946 (2012).
4. Vogelsberger, M. *et al.* Introducing the Illustris Project: simulating the coevolution of dark and visible matter in the Universe. *Mon. Not. R. Astron. Soc.* **444,** 1518–1547 (2014).
5. Schaye, J. *et al.* The EAGLE project: simulating the evolution and assembly of galaxies and their environments. *Mon. Not. R. Astron. Soc.* **446,** 521–554 (2015).
6. Choi, E. *et al.* Physics of galactic metals: evolutionary effects due to production, distribution, feedback & interaction with black holes. *Astrophys. J.* **844,** 31 (2016).
7. Ferrarese, L. & Merritt, D. A fundamental relation between supermassive black holes and their host galaxies. *Astrophys. J.* **539,** L9–L12 (2000).
8. Crain, R. A. *et al.* The EAGLE simulations of galaxy formation: calibration of subgrid physics and model variations. *Mon. Not. R. Astron. Soc.* **450,** 1937–1961 (2015).
9. Sijacki, D. *et al.* The Illustris simulation: the evolving population of black holes across cosmic time. *Mon. Not. R. Astron. Soc.* **452,** 575–596 (2015).
10. van den Bosch, R. C. E., Gebhardt, K., Gültekin, K., Yldrm, A. & Walsh, J. L. Hunting for supermassive black holes in nearby galaxies with the Hobby–Eberly Telescope. *Astrophys. J. Suppl. Ser.* **218,** 10 (2015).
11. Rodriguez-Gomez, V. *et al.* The stellar mass assembly of galaxies in the Illustris simulation: growth by mergers and the spatial distribution of accreted stars. *Mon. Not. R. Astron. Soc.* **458,** 2371–2390 (2016).
12. van den Bosch, R. C. E. Unification of the fundamental plane and super massive black hole masses. *Astrophys. J.* **831,** 134 (2016).
13. Ocvirk, P., Pichon, C., Lançon, A. & Thiébaut, E. STECKMAP: STEllar Content and Kinematics from high resolution galactic spectra via Maximum A Posteriori. *Mon. Not. R. Astron. Soc.* **365,** 74–84 (2006).
14. Vazdekis, A. *et al.* Evolutionary stellar population synthesis with MILES—I. The base models and a new line index system. *Mon. Not. R. Astron. Soc.* **404,** 1639–1671 (2010).
15. Koleva, M., Prugniel, P., Ocvirk, P., Le Borgne, D. & Soubiran, C. Spectroscopic ages and metallicities of stellar populations: validation of full spectrum fitting. *Mon. Not. R. Astron. Soc.* **385,** 1998–2010 (2008).
16. Sánchez-Blázquez, P., Ocvirk, P., Gibson, B. K., Pérez, I. & Peletier, R. F. Star formation history of barred disc galaxies. *Mon. Not. R. Astron. Soc.* **415,** 709–731 (2011).
17. Leitner, S. N. On the last 10 billion years of stellar mass growth in star-forming galaxies. *Astrophys. J.* **745,** 149 (2012).
18. Ruiz-Lara, T. *et al.* Recovering star formation histories: Integrated-light analyses vs. stellar colour-magnitude diagrams. *Astron. Astrophys.* **583,** A60 (2015).
19. Beifiori, A., Courteau, S., Corsini, E. M. & Zhu, Y. On the correlations between galaxy properties and supermassive black hole mass. *Mon. Not. R. Astron. Soc.* **419,** 2497–2528 (2012).
20. Thomas, D., Maraston, C., Bender, R. & Mendes de Oliveira, C. The epochs of early-type galaxy formation as a function of environment. *Astrophys. J.* **621,** 673–694 (2005).
21. Peng, C. Y. How mergers may affect the mass scaling relation between gravitationally bound systems. *Astrophys. J.* **671,** 1098–1107 (2007).
22. Jahnke, K. & Macciò, A. V. The non-causal origin of the black-hole-galaxy scaling relations. *Astrophys. J.* **734,** 92 (2011).
23. Fan, X. *et al.* A survey of $z>5.8$ quasars in the Sloan Digital Sky Survey. I. Discovery of three new quasars and the spatial density of luminous quasars at $z=6$. *Astron. J.* **122,** 2833–2849 (2001).
24. Martin-Navarro, I., Brodie, J. P., van den Bosch, R. C. E., Romanowsky, A. J. & Forbes, D. A. Stellar populations across the black hole mass-velocity dispersion relation. *Astrophys. J.* **832,** L11 (2016).
25. Terrazas, B. A. *et al.* Quiescence correlates strongly with directly measured black hole mass in central galaxies. *Astrophys. J.* **830,** L12 (2016).
26. Bower, R. G. *et al.* The dark nemesis of galaxy formation: why hot haloes trigger black hole growth and bring star formation to an end. *Mon. Not. R. Astron. Soc.* **465,** 32–44 (2017).
27. Kauffmann, G. *et al.* The host galaxies of active galactic nuclei. *Mon. Not. R. Astron. Soc.* **346,** 1055–1077 (2003).
28. Mullaney, J. R. *et al.* GOODS-Herschel: the far-infrared view of star formation in active galactic nucleus host galaxies since $z\approx3$. *Mon. Not. R. Astron. Soc.* **419,** 95–115 (2012).
29. Stanley, F. *et al.* A remarkably flat relationship between the average star formation rate and AGN luminosity for distant X-ray AGN. *Mon. Not. R. Astron. Soc.* **453,** 591–604 (2015).
30. Ruschel-Dutra, D., Rodríguez Espinosa, J. M., González Martín, O., Pastoriza, M. & Riffel, R. Star formation in AGNs at the hundred parsec scale using MIR high-resolution images. *Mon. Not. R. Astron. Soc.* **466,** 3353–3363 (2017).

Acknowledgements We acknowledge support from the National Science Foundation (NSF) grants AST-1616598 and AST-1616710, from a Marie Curie Global Fellowship, from SFB 881 'The Milky Way System' (subprojects A7 and A8) funded by the German Research Foundation, and from grants AYA2016-77237-C3-1-P and AYA2014-56795-P from the Spanish Ministry of Economy and Competitiveness (MINECO). G.v.d.V. acknowledges funding from the European Research Council (ERC) under the European Union's Horizon 2020 research and innovation programme under grant agreement no. 724857 (Consolidator Grant ArcheoDyn). A.J.R. was supported as a Research Corporation for Science Advancement Cottrell Scholar. I.M.-N. thanks the TRACES group and M. Mezcua for their comments, R. van den Bosch for making the HETMGS data publicly available and A. Boecker for her help.

Author Contributions I.M.-N. derived the star formation histories along with T.R.-L. and wrote the text. J.P.B., A.J.R., T.R.-L. and G.v.d.V. contributed to the interpretation and analysis of the results.

Author Information Reprints and permissions information is available at www.nature.com/reprints. The authors declare no competing financial interests. Readers are welcome to comment on the online version of the paper. Publisher's note: Springer Nature remains neutral with regard to jurisdictional claims in published maps and institutional affiliations. Correspondence and requests for materials should be addressed to I.M.-N. (imartinn@ucsc.edu).

Reviewer Information *Nature* thanks D. Rosario, J. Trump and the other anonymous reviewer(s) for their contribution to the peer review of this work.

METHODS

Data quality and spectral fitting. Representative spectra of a low-σ and a high-σ galaxy are shown in Extended Data Fig. 1, with the best-fitting STECKMAP model overplotted. Because of the high signal-to-noise ratio of the data (typically above about 100 $Å^{-1}$), the residuals are typically below 1% (approximately 0.06 and 0.08 for these low-σ and high-σ objects, respectively).

Velocity dispersion–metallicity degeneracy. There is a well-known degeneracy between σ and galaxy metallicity[15], which could potentially affect our measurements of the SFH. It has been shown that fitting kinematics and stellar population properties independently minimizes the effect of this degeneracy[16]. Thus, we first determined the kinematics (systemic velocity V_{sys} and σ) using the penalized pixel-fitting method (pPXF)[31], which was also used to remove the nebular emission from our spectra. The temporal combination of models of single stellar populations. convolved to the resolution of the galaxy measured with pPXF, was used to calculate the SFHs.

As a further test to assess the dependence of our results on the adopted velocity dispersion, we repeated the analysis while allowing STECKMAP to measure the kinematics at the same time as the SFHs, although this approach has been proved to be less accurate[16]. In Extended Data Fig. 2, we show the cumulative mass distributions of under-massive and over-massive black-hole galaxies measured in this way. The observed differences in the SFHs across the relation between black-hole mass and σ are not due to degeneracies between stellar populations and kinematical properties.

Robustness of the results. *Regularization parameters.* To assess the robustness of our results, we varied the two main free parameters in our analysis. On the one hand, STECKMAP allows for a regularization in both the SFH (μ_x) and the age–metallicity relation (μ_Z) of the different stellar population models. Effectively, this regularization behaves as a Gaussian prior[32]. Figure 2 was calculated using $\mu_x = \mu_Z = 10$. Although the choice of these parameters mainly depends on the quality and characteristics of the observed spectra, we repeated the analysis but varying each regularization parameter by two orders of magnitude. In Extended Data Fig. 3, we demonstrate that our choice of the regularization parameters does not affect the main conclusions of this work but provides the most stable solutions within the range of μ_x and μ_Z values explored.

Sample selection. As described in the main text, the final sample consists of every galaxy in the HETMGS survey with good enough spectra to perform our stellar population analysis. In practice, this means rejecting spectra with very low signal-to-noise ratio (less than about 10) and strong emission lines. Possible biases related to these selection criteria are discussed below. No additional constraints were applied. Our best-fitting relation is based on our own determinations of the velocity dispersion of individual galaxies, homogeneously measured at half R_e. Galaxies with black-hole masses departing from our best-fitting $M_\bullet$–σ by more than +0.2 or −0.2 dex were classified as over-massive or under-massive black-hole galaxies, respectively. With this criterion, the number of over-massive, standard and under-massive black-hole galaxies is similar, at 25, 24 and 25 objects, respectively. As reported in previous studies of large sample of black-hole masses[12,19], there is no morphological dependence of our best-fitting $M_\bullet$–σ relation. In Extended Data Fig. 4, we show the distributions for the concentration parameter $C_{28} \equiv 5\log(R_{80}/R_{20})$ for under-massive and over-massive black-hole galaxies. Galactocentric distances R_{80} and R_{20} encompass 80% and 20% of the total light of the galaxy, respectively, and were measured using elliptical isophotes[12]. The parameter C_{28} is a proxy for the light concentration of galaxies and therefore of their morphology. Higher C_{28} corresponds to ellipsoids, whereas lower values are associated with galaxies that are more disk-like[33,34]. As expected, C_{28} behaves similarly across the $M_\bullet$–σ relation, with median values of 5.5 and 5.6 for over-massive and under-massive black-hole galaxies, respectively. A two-sided Kolmogorov–Smirnov test indicates that the differences between the two C_{28} distributions are insignificant ($P = 0.82$). Thus, over-massive black-hole galaxies are morphologically indistinguishable from under-massive black-hole objects.

We also investigated whether the assumed best-fitting $M_\bullet$–σ relation could lead to spurious results. As an extreme test, we recalculated the mean SFHs but, instead of using our best-fitting solution, we assumed the one calculated for a much larger sample of black-hole masses[12]. This sample includes objects that were not observed by HETMGS or whose spectra were rejected in our analysis because of the poor quality. Specifically, this alternative $M_\bullet$–σ relation is given by $\log M_\bullet = -4.00 + 5.35\log\sigma$. Note that the use of this equation is not consistent with our sample. Velocity dispersions were calculated differently and over different radial apertures ($0.5R_e$ versus $1R_e$). Thus, adopting this equation to distinguish between over-massive and under-massive black-hole galaxies could potentially affect our conclusions. Despite this, Extended Data Fig. 3 shows that the dependence of the SFH on the mass of the central black hole stands, regardless of the implicit $M_\bullet$–σ relation.

It is worth noting that the zero point and the slope of the $M_\bullet$–σ relation depend on the effective velocity dispersion of individual galaxies and, to a lesser extent, on the assumed mass of the black hole. Whereas the latter is unambiguously defined, the stellar velocity dispersion varies considerably within galaxies. However, the relative distinction between over-massive and under-massive black-hole galaxies is relatively insensitive to the characteristics of different samples. The majority of objects (about 85%) classified as over-massive or under-massive using our best-fitting relation are also over-massive or under-massive according to other widely adopted $M_\bullet$–σ relations[12,35]. Thus, our classification and therefore our conclusions do not depend on absolute σ values.

Finally, we have also considered the possibility that differences in the internal kinematics or morphology of galaxies could bias our conclusions. In particular, under-massive black-hole galaxies may be offset from the average $M_\bullet$–σ relation owing to a higher prevalence of disk-like, rotationally supported structures, which in general tend to show younger populations[36]. Observationally, there is no evidence of a morphological or mass-concentration dependency of the $M_\bullet$–σ relation[19], although it has been claimed that pseudo-bulges may follow a different scaling relation[19,37,38], which becomes relevant for velocity dispersions $\sigma < 200\,\mathrm{km\,s^{-1}}$. In Extended Data Fig. 5, we show the star formation rate as a function of look-back time only for galaxies above this velocity dispersion threshold, where the bulk of the population is dispersion-supported. It is clear that the observed differences in the star formation processes between over-massive and under-massive black-hole galaxies are not due to a morphological or kinematical effect.

Nebular emission and young stellar populations. Although the age sensitivity of the spectra is widely spread over the whole wavelength range[32], our strongest age-sensitive feature is the Hβ line. Thus, we decided to be conservative and remove from the analysis objects with strong emission lines (amplitude-to-noise ratio > 4), which effectively leads to the old stellar populations shown in Fig. 2. If we include galaxies with stronger emission lines, STECKMAP recovers the expected contribution of younger stars, without softening the differences between over-massive and under-massive black-hole galaxies, as shown in Extended Data Fig. 6.

Stellar population synthesis models. The main source of systematic uncertainties in any stellar population analysis is the choice of a given set of models. We used the MILES stellar population models as a reference, as they provide fully empirical spectroscopic predictions over the explored wavelength range and are best suited for intermediate-to-old stellar populations[14]. However, given our relatively narrow coverage of wavelengths, we also addressed the impact of the choice of stellar population model on our results. We repeated the analysis of our sample of galaxies but considering three additional sets of models, namely the PÉGASE-HR model[39], the Bruzual and Charlot 2003 (BC03) model[40] and the GRANADA/MILES model[41,42]. As shown in Extended Data Fig. 7, the differences between over-massive and under-massive black-hole galaxies are clear in all three models. The agreement between different models is remarkable given the strong underlying differences among them. As an additional test of the robustness of our analysis, we also compared our observations to a new set of the MILES models which make use of BaSTi isochrones[43]. This final comparison is also included in Extended Data Fig. 7, further reinforcing the conclusion that our results are not driven by systematics in the stellar population analysis.

Galaxy densities and sample biases. The statistical properties of galaxies with measured black-hole masses do not follow those of the overall population of galaxies. In particular, objects with known black-hole masses tend to be denser than the average[10,44], partially because our ability to measure black-hole masses depends on how well we can resolve their spheres of influence[45]. To test whether density is a confounding variable in our analysis, we performed a bilinear fitting between $M_\bullet$–σ and stellar density ($M_\star/R_e^3$). We used publicly available measurements of sizes (R_e) and K-band luminosities[12] to obtain a best-fitting relation given by

$$\log M_\bullet = -1.5 + 4.42\log\sigma - 0.05\log(M_\star R_e^{-3}) \quad (1)$$

where $M_\star$ is the stellar mass based on the K-band luminosity and R_e the effective radius. This best-fitting relation, consistent with previous studies[46] (Extended Data Fig. 8), allowed us to investigate the effect of the black hole at fixed stellar velocity dispersion and density. This relation is still mostly driven by σ and only weakly depends on stellar density. The cumulative mass distribution of over-massive and under-massive black-hole galaxies, according to the equation above, is shown in Extended Data Fig. 8. We found that, when stellar density is also taken into account, the decoupling between over-massive and under-massive black-hole galaxies remains unaltered. Thus, the differences observed in the SFHs are not due to different galaxy densities. Selection biases in the current sample of black-hole masses would, if anything[47], change only the normalization of the $M_\bullet$–σ relation[45]. Our approach, by construction, is insensitive to this effect.

Additionally, we explored possible bias introduced by our rejection criteria—that is, those galaxies that we did not include in the analysis either because of low signal-to-noise ratio or because of strong emission features. In Extended Data Fig. 9, we show the R_e–σ distribution for HETMGS galaxies, for which the sizes were taken from the 2MASS Extended Source catalogue[48], averaged following the method adopted by the ATLAS^{3D} team[49]. We used the stellar velocity dispersions listed in the HETMGS presentation paper[10]. The typical sizes of over-massive and under-massive black-hole galaxies ($R_e^{OM} = 2.69 \pm 0.34$ kpc and $R_e^{UM} = 2.49 \pm 0.37$ kpc, respectively) are consistent with the average population of galaxies with known black-hole masses ($R_e^{BH} = 2.74 \pm 0.22$ kpc). The same applies to the K-band luminosities, with a typical value of $\log(L_K^{OM}/L_\odot) = 11.13 \pm 0.08$, $\log(L_K^{UM}/L_\odot) = 11.05 \pm 0.07$ and $\log(L_K^{BH}/L_\odot) = 11.08 \pm 0.05$, for over-massive black-hole galaxies, under-massive black-hole galaxies and the complete sample of black-hole galaxies, respectively. We therefore conclude that our final sample is not significantly biased relative to the average population of galaxies with measured black-hole masses.

Code availability. The STECKMAP code used to derive the SFHs is publicly available at http://astro.u-strasbg.fr/~ocvirk/indexsteckmap.html.

Data availability. All data analysed during this study are available at the HETMGS website http://www.mpia.de/~bosch/hetmgs/.

31. Cappellari, M. & Emsellem, E. Parametric recovery of line-of-sight velocity distributions from absorption-line spectra of galaxies via penalized likelihood. *Publ. Astron. Soc. Pacif.* **116,** 138–147 (2004).
32. Ocvirk, P., Pichon, C., Lançon, A. & Thiébaut, E. STECMAP: STEllar Content from high-resolution galactic spectra via Maximum A Posteriori. *Mon. Not. R. Astron. Soc.* **365,** 46–73 (2006).
33. Shimasaku, K. *et al.* Statistical properties of bright galaxies in the Sloan Digital Sky Survey Photometric System. *Astron. J.* **122,** 1238–1250 (2001).
34. Courteau, S., McDonald, M., Widrow, L. M. & Holtzman, J. The bulge–halo connection in galaxies: a physical interpretation of the V_c–σ_0 relation. *Astrophys. J.* **655,** L21–L24 (2007).
35. Kormendy, J. & Ho, L. C. Coevolution (or not) of supermassive black holes and host galaxies. *Annu. Rev. Astron. Astrophys.* **51,** 511–653 (2013).
36. Kuntschner, H. *et al.* The SAURON project: XVII. Stellar population analysis of the absorption line strength maps of 48 early-type galaxies. *Mon. Not. R. Astron. Soc.* **408,** 97–132 (2010).
37. Hu, J. The black hole mass–stellar velocity dispersion correlation: bulges versus pseudo-bulges. *Mon. Not. R. Astron. Soc.* **386,** 2242–2252 (2008).
38. Kormendy, J., Bender, R. & Cornell, M. E. Supermassive black holes do not correlate with galaxy disks or pseudobulges. *Nature* **469,** 374–376 (2011).
39. Le Borgne, D. *et al.* Evolutionary synthesis of galaxies at high spectral resolution with the code PEGASE-HR. Metallicity and age tracers. *Astron. Astrophys.* **425,** 881–897 (2004).
40. Bruzual, G. & Charlot, S. Stellar population synthesis at the resolution of 2003. *Mon. Not. R. Astron. Soc.* **344,** 1000–1028 (2003).
41. González Delgado, R. M., Cerviño, M., Martins, L. P., Leitherer, C. & Hauschildt, P. H. Evolutionary stellar population synthesis at high spectral resolution: optical wavelengths. *Mon. Not. R. Astron. Soc.* **357,** 945–960 (2005).
42. González Delgado, R. M. & Cid Fernandes, R. Testing spectral models for stellar populations with star clusters: II. Results. *Mon. Not. R. Astron. Soc.* **403,** 797–816 (2010).
43. Pietrinferni, A., Cassisi, S., Salaris, M. & Castelli, F. A large stellar evolution database for population synthesis studies. I. Scaled solar models and isochrones. *Astrophys. J.* **612,** 168–190 (2004).
44. Bernardi, M., Sheth, R. K., Tundo, E. & Hyde, J. B. Selection bias in the $M_\bullet$–σ and $M_\bullet$–L correlations and its consequences. *Astrophys. J.* **660,** 267–275 (2007).
45. Shankar, F. *et al.* Selection bias in dynamically measured supermassive black hole samples: its consequences and the quest for the most fundamental relation. *Mon. Not. R. Astron. Soc.* **460,** 3119–3142 (2016).
46. Saglia, R. P. *et al.* The SINFONI Black Hole Survey: the black hole fundamental plane revisited and the paths of (co)evolution of supermassive black holes and bulges. *Astrophys. J.* **818,** 47 (2016).
47. Gültekin, K., Tremaine, S., Loeb, A. & Richstone, D. O. Observational selection effects and the M–σ relation. *Astrophys. J.* **738,** 17 (2011).
48. Jarrett, T. H. *et al.* 2MASS Extended Source Catalog: overview and algorithms. *Astron. J.* **119,** 2498–2531 (2000).
49. Cappellari, M. *et al.* The ATLAS^{3D} project: I. A volume-limited sample of 260 nearby early-type galaxies: science goals and selection criteria. *Mon. Not. R. Astron. Soc.* **413,** 813–836 (2011).

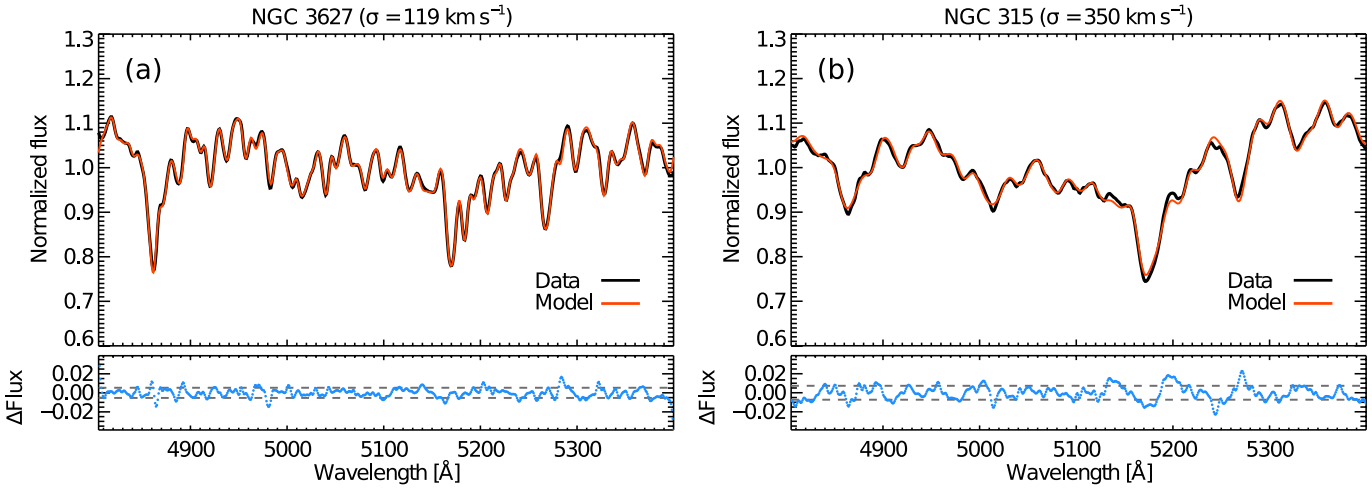

Extended Data Figure 1 | Data and best-fitting stellar populations model. a, The spectrum of the low-σ galaxy NGC 3627; **b**, the spectrum of the higher-σ galaxy NGC 315. Along with the HETMGS spectra (black line), we also show the best-fitting STECKMAP model (red line). In the bottom panel, we show the residuals (blue dots), which are in both cases below 2%. The standard deviation is shown as dashed horizontal lines.

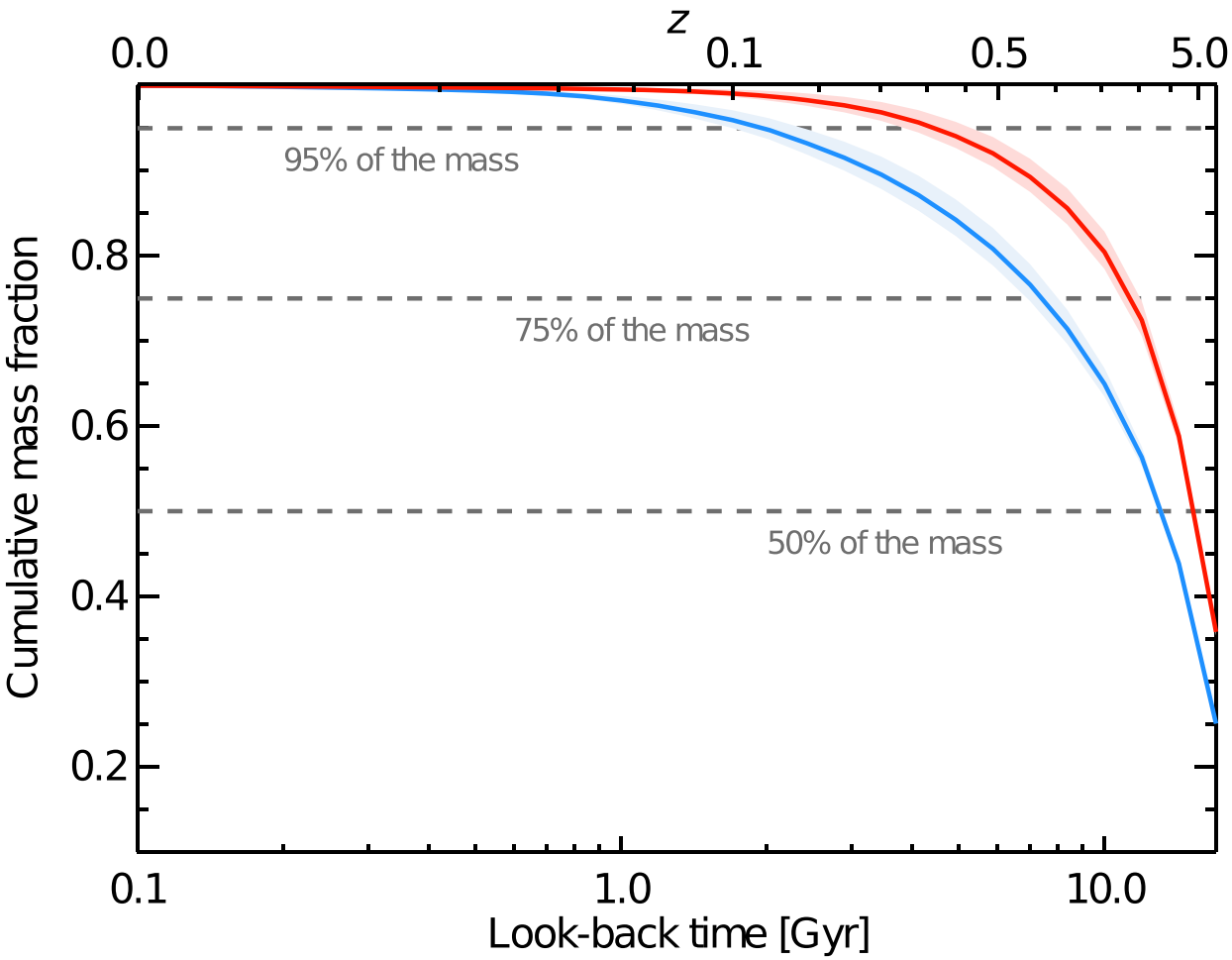

Extended Data Figure 2 | Cumulative mass distributions without fixing the kinematics. To assess the degeneracy between stellar population properties and stellar velocity dispersion, we repeated the analysis while allowing STECKMAP to fit the kinematics simultaneously with the SFHs. In red and blue, the cumulative mass fractions of under-massive (blue) and over-massive (red) black-hole galaxies are shown as a function of look-back time. Although leaving the kinematics as free parameters leads to less accurate SFHs[16], the differences in the star formation of under-massive and over-massive black-hole galaxies remain clear.

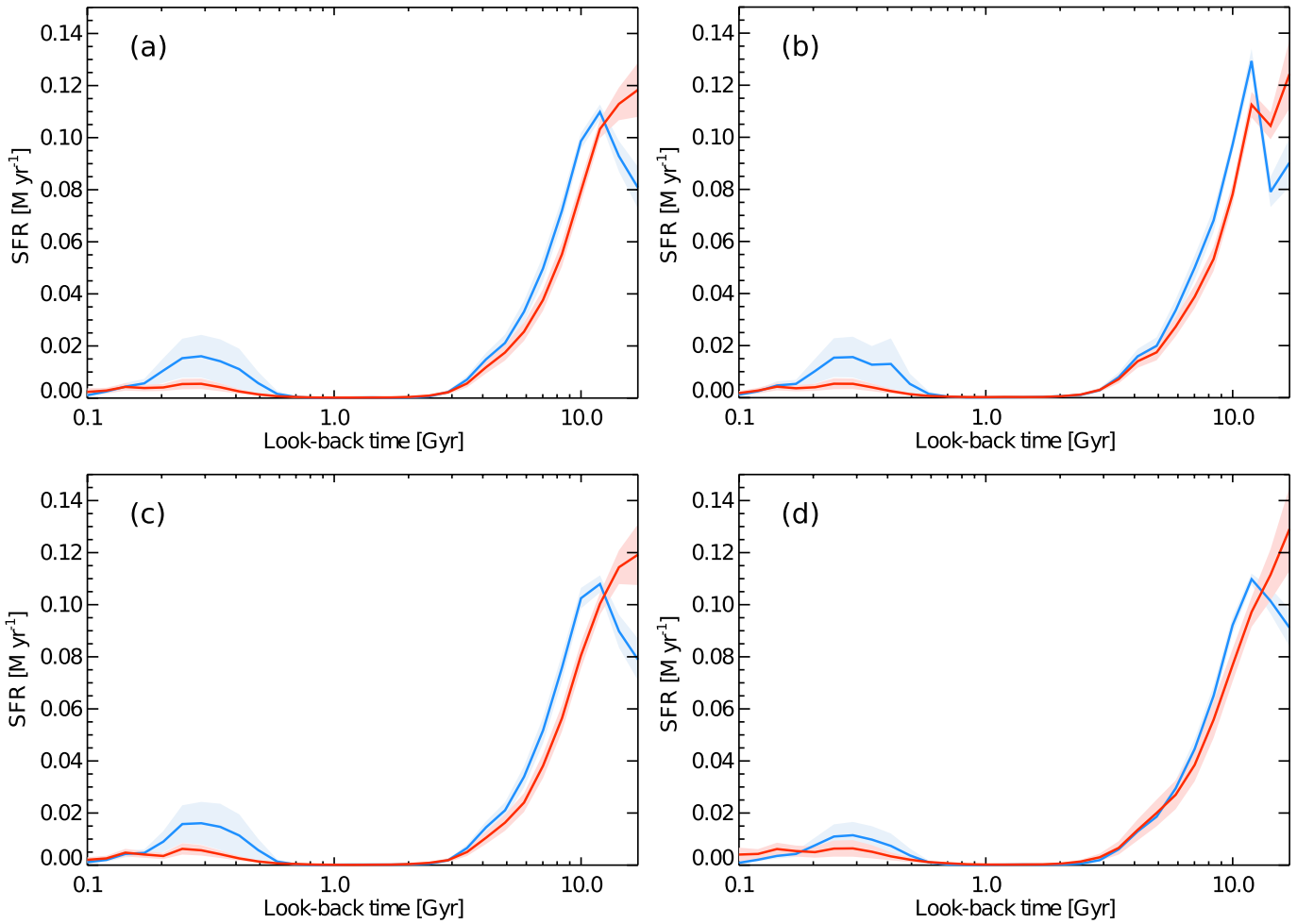

Extended Data Figure 3 | Robustness of the recovered star formation rates. Different panels correspond to the different tests performed in order to explore the reliability of our results. As in Fig. 2, red and blue lines indicate the star formation rate (SFR) as a function of look-back time for over-massive and under-massive black-hole galaxies, and the shaded areas mark the 1σ uncertainties. **a**, Our preferred model, as a reference. A two-sided Kolmogorov–Smirnov comparison between over-massive and under-massive galaxies indicates that the two distributions are significantly different ($P = 0.026$). **b**, Here, we left the regularization of the SFH almost free, by setting $\mu_x = 0.1$. **c**, We varied the regularization of the age–metallicity relation in the same way, changing μ_Z from 10 to 0.1. **d**, Finally, we adopted a different (but inconsistent) $M_\bullet$–σ relation[12] to separate our sample. All these tests demonstrate that our conclusions are insensitive to systematics in the analysis.

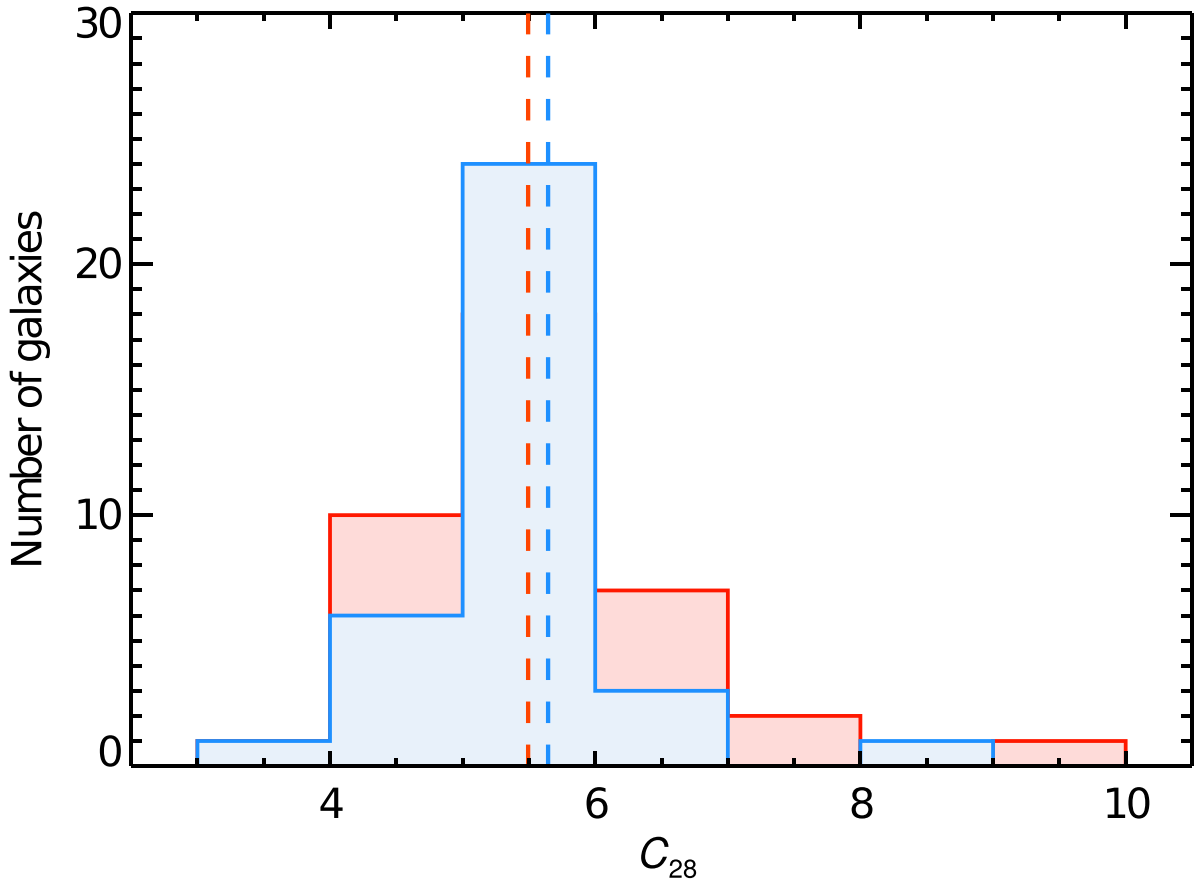

Extended Data Figure 4 | Distributions of concentration parameters. The distribution of the C_{28} concentration parameter is shown in red and blue for over-massive and under-massive black-hole galaxies, respectively. Higher (lower) concentration indices are associated with earlier (later) morphological types. Vertical dashed lines mark the median of the distributions. No significant differences are found between the samples, indicating that the over-massive and under-massive black-hole galaxies are morphologically indistinguishable. This suggests that both types of galaxy share the same formation processes but differ in the present-day mass of their central black holes.

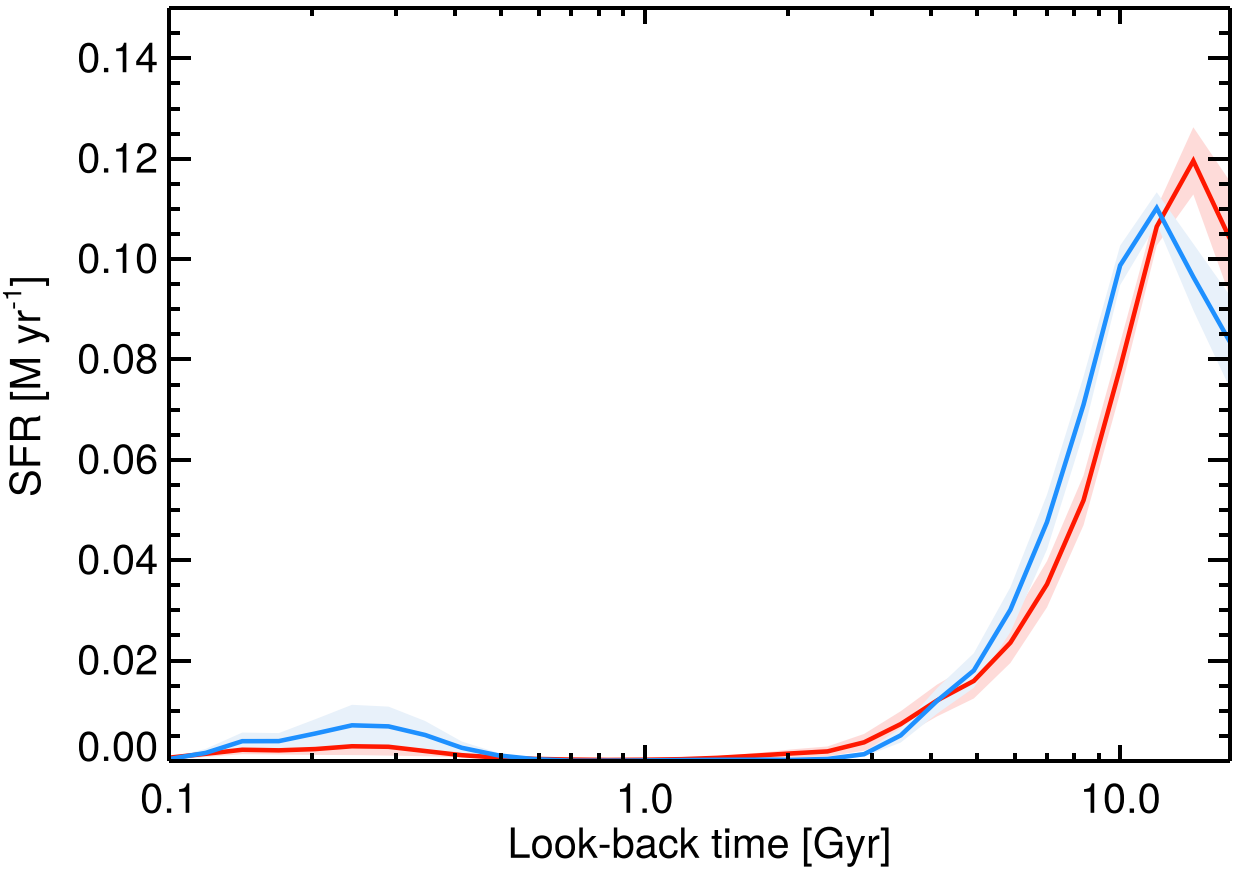

Extended Data Figure 5 | Star formation rate for high-mass galaxies. Differences in the star formation rate as a function of look-back time for over-massive (red) and under-massive (blue) black-hole galaxies, but only including objects with velocity dispersions $\sigma > 200\,\mathrm{km\ s^{-1}}$ ($\log\sigma = 2.32$). The massive end of the $M_\bullet$–σ relation is dominated by elliptical, pressure-supported systems[12,19] but shows the same distinction between over-massive and under-massive black-hole galaxies.

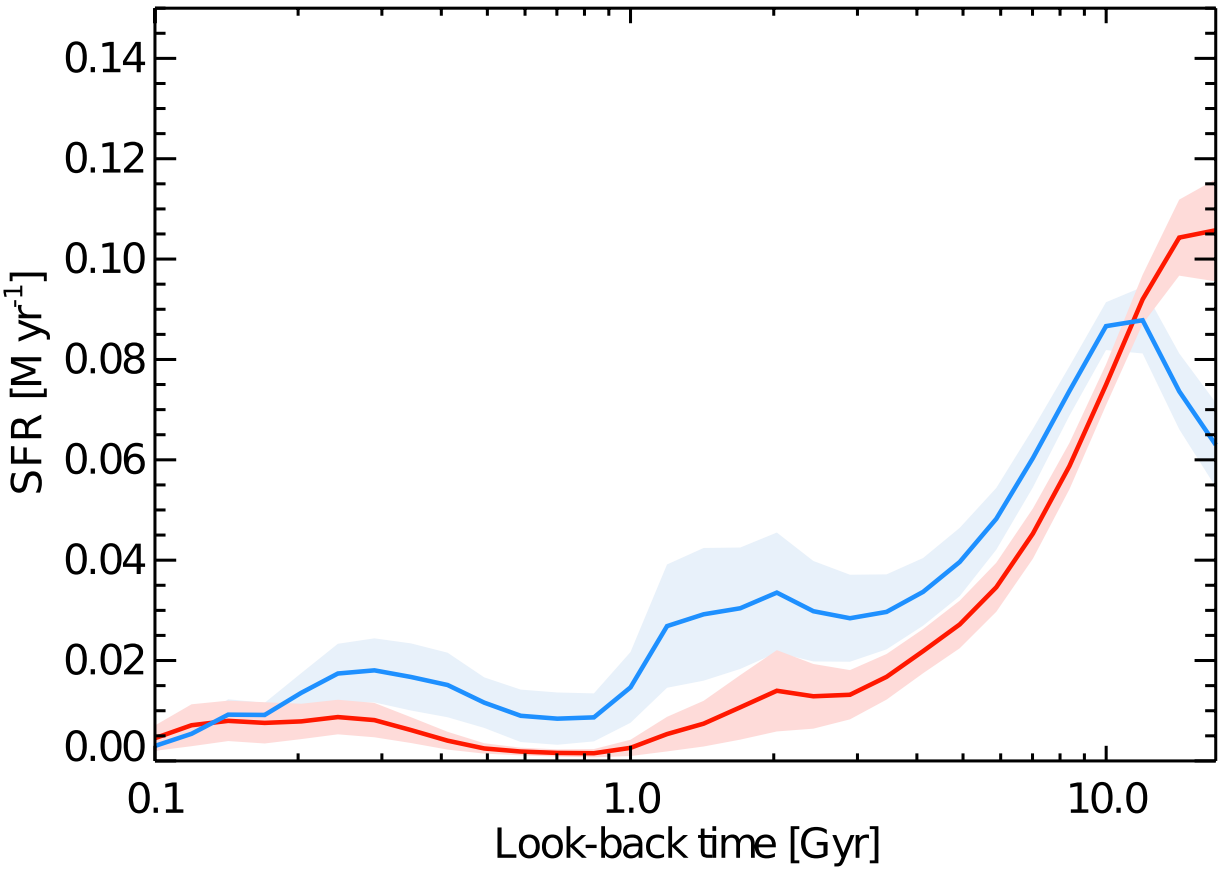

Extended Data Figure 6 | Nebular emission and star formation rate. If we include galaxies with strong emission lines in the analysis, the quality of the fits worsens but over-massive (red) and under-massive (blue) black-hole galaxies still show decoupled SFHs.

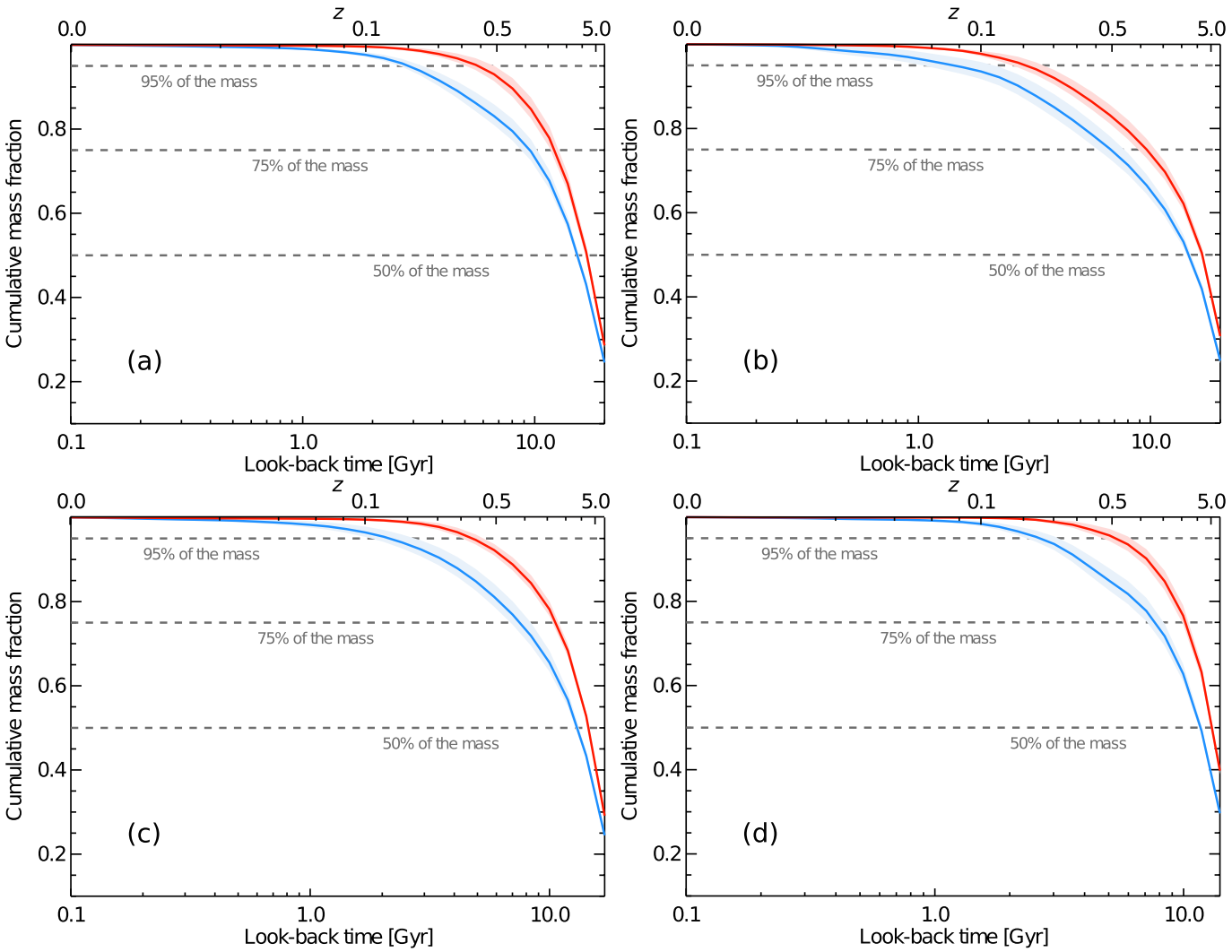

Extended Data Figure 7 | Dependence on the stellar population models. As in Fig. 2, each panel shows the cumulative mass fraction for over-massive (red) and under-massive (blue) black-hole galaxies. In each panel, the SFHs were calculated using a different set of stellar population synthesis models. **a**, Result based on the PÉGASE-HR[39] models; **b**, result based BC03 model[40]; **c**, result using the GRANADA/MILES models[41,42]; **d**, finally, result using the MILES models with BaSTi isochrones[43]. Despite the quantitative differences, the different behaviour of under-massive and over-massive black-hole galaxies is clear in all panels, and thus it is not an artefact of a particular set of models. Note that different models are fed with different stellar libraries, interpolated in different ways to populate different isochrones. The separation between over-massive and under-massive black-hole galaxies is thus independent of the different ingredients in stellar population modelling.

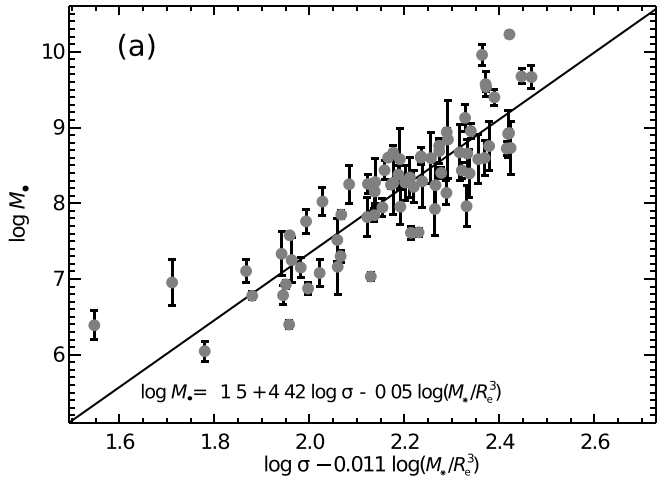

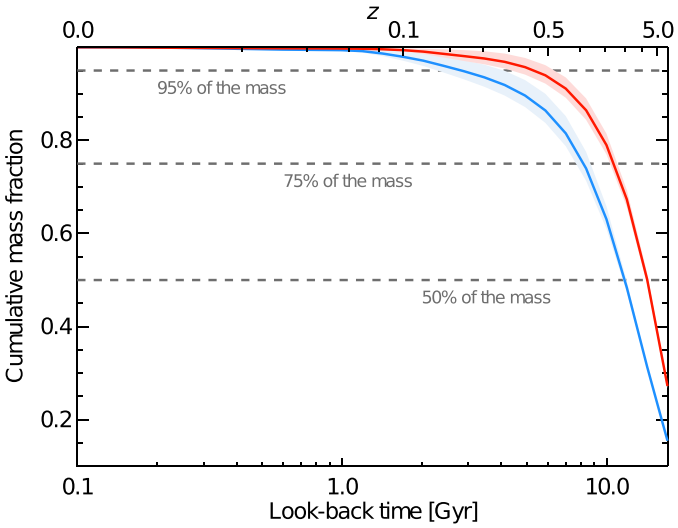

Extended Data Figure 8 | Stellar density as a confounding variable. **a**, $M_\bullet$ as a function of the best-fitting combination of σ and stellar density, following equation (1). Projecting over this plane allows us to separate galaxies depending on the mass of their black holes, but at fixed stellar velocity dispersion and stellar density (M_*/R_e^3). **b**, The cumulative mass distributions of over-massive and under-massive black-hole galaxies according to this new definition. This test demonstrates that the observed differences in the SFHs are not due to a possible variation of the stellar density across the $M_\bullet$–σ relation, further supporting the role of the black hole in regulating star formation within massive galaxies.

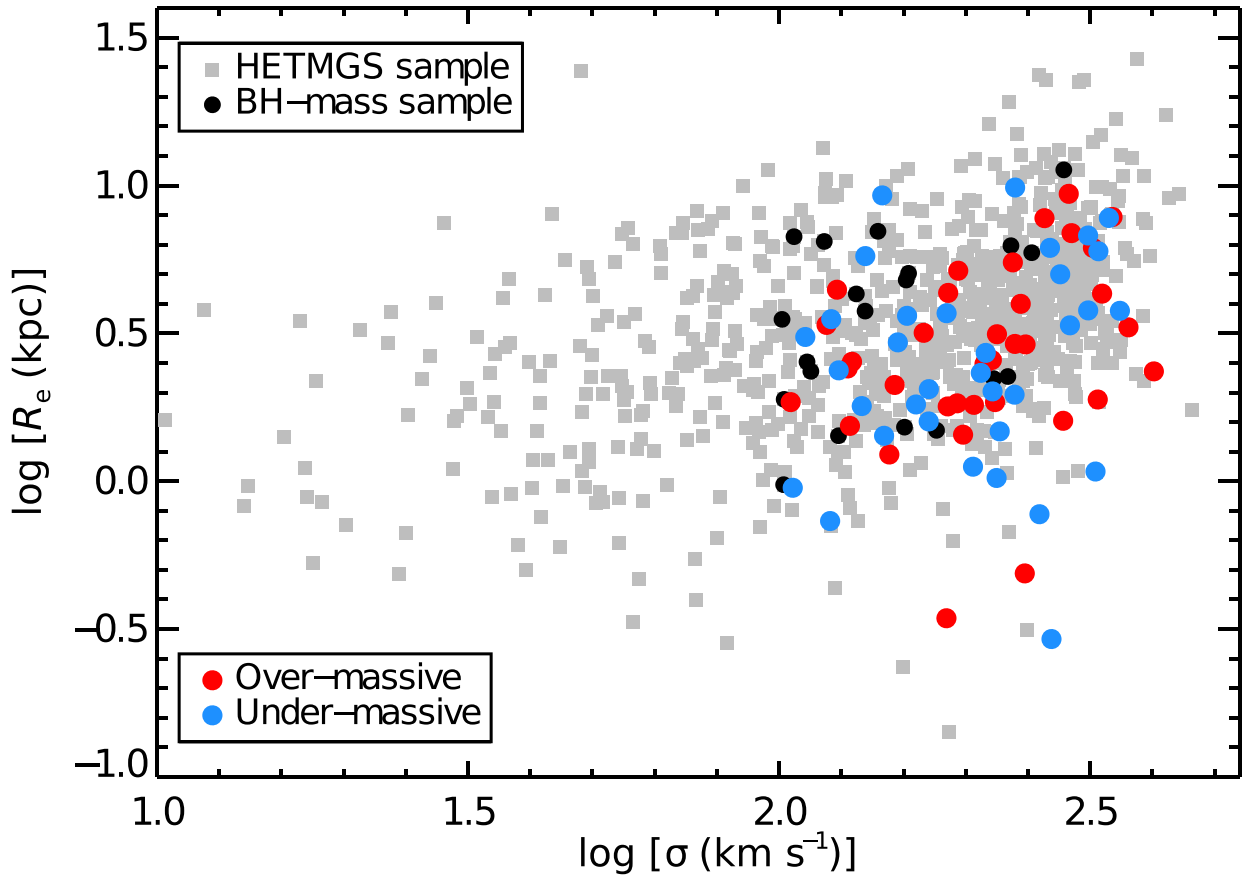

Extended Data Figure 9 | Selection function. Filled grey squares show the size–σ relation for the HETMGS sample, and filled circles correspond to those galaxies with measured black-hole masses (blue and red indicate under-massive and over-massive, respectively), which are, on average, more compact than the overall population. However, we found no differences in the mean sizes of our final sample of galaxies (both over-massive and under-massive), compared with the total population of galaxies with known black-hole masses (filled circles). Thus, our results are not driven by our rejection criteria in terms of signal-to-noise ratio or emission-line contamination.